Applied Catalysis B: Environment and Energy 346 (2024) 123719

Contents lists available at ScienceDirect

Applied Catalysis B: Environment and Energy

journal homepage: www.elsevier.com/locate/apcatb

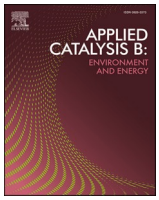

A switchable hydrogenation chemoselectivity of biomass platform compounds based on solvent regulation

Yuanjing Zhang [a,1], Si Wang [a,1], Yusen Yang [a,b,*], Lei Wang [a,b], Enze Xu [a], Quandong Hou [a], Shiquan Zhao [a], Tianyong Liu [a], Song Hong [a], Lirong Zheng [c], Feng Li [a], Xin Zhang [a,b,*], Min Wei [a,b,*]

[a] State Key Laboratory of Chemical Resource Engineering, Beijing Advanced Innovation Center for Soft Matter Science and Engineering, Beijing University of Chemical Technology, Beijing 100029, PR China
[b] Quzhou Institute for Innovation in Resource Chemical Engineering, Quzhou 324000, PR China
[c] Institute of High Energy Physics, Chinese Academy of Sciences, Beijing 100049, PR China

ARTICLE INFO

Keywords:
Solvent effect
Selective hydrogenation
Fully exposed cluster catalyst
Adsorption configuration
Structure-selectivity relationship

ABSTRACT

Selective catalytic conversion of biomass-derived compounds to fuels and fine chemicals serves as a renewable energy pathway for the partial substitution of fossil resources, in which reaction pathway and selectivity control are key issues. Herein, we report a fully exposed Pt clusters immobilized on CoAl mixed metal oxides catalyst (denoted as Pt_n/CoAl-MMOs), which exhibits prominent catalytic performance towards liquid phase hydrogenation reaction of furfural (FAL). Noteworthily, the hydrogenation chemoselectivity can be switched among four products *via* using four different solvents: tetrahydrofurfuryl alcohol (THFA; yield: 91.4%), furfuryl alcohol (FA; yield: 97.7%), 2-methylfuran (2-MF; yield: 92.1%) and furan (FU; yield: 90.8%) are obtained in ethanol, dioxane, isopropanol and *n*-hexane solvent, respectively. Experimental studies (*in situ* FT-IR and TPSR-Mass) combined with theoretical calculations (DFT) reveal that solvent molecules exert an essential influence on the adsorption configuration of FAL *via* changing the solvent-catalyst and/or substrate-catalyst interaction, which ultimately determines the hydrogenation pathway, key intermediate and final product. This work demonstrates a facile solvent-dependent product-switching strategy within one catalytic system, which opens up potential opportunities for tailoring hydrogenation selectivity in liquid-solid catalytic reactions towards biomass upgrading.

1. Introduction

With the increasing crisis of fossil resources and environmental problems, as a kind of beneficial renewable and sustainable resource, the effective conversion and utilization of biomass resources have aroused intensive interest of researchers [1–4]. Selective hydrogenation of biomass-derived compounds to produce fine chemicals and value-added fuels occupies a prominent position in advancing the utilization of renewable energy resources [5–7]. Furfural (FAL), a prominent biomass-derived platform molecule produced from lignocellulose, serves as a pivotal link connecting biomass feedstock and versatile chemicals and biofuels [8,9]. FAL is a highly unsaturated compound featuring conjugate C═C and C═O bonds as well as a furan heterocycle, which can be directly or indirectly converted to various high value-added down-stream products. For instance, tetrahydrofurfuryl alcohol (THFA) is an important eco-friendly solvent applied in the realms of agriculture and the printing industry [10]; furfuryl alcohol (FA) finds extensive applications in the production of vitamins, resin, lubricating oils and lysine [11]; 2-methylfuran (2-MF) possesses a high octane rating and low water solubility, making itself a viable fuel additive for gasoline [12]; whilst furan (FU) is generally used in many organic synthesis (*e.g.*, pyrrole, thiophene and drugs) [13]. The hydrogenation of FAL involves an integrated and complicated reaction network, and it is highly desirable to manipulate the chemoselective conversion of FAL towards each target product. However, the switchable conversion of FAL into multitarget products within a single catalytic reaction system remains a huge challenge.

For the catalytic hydrogenation reactions, the current research

* Corresponding authors at: State Key Laboratory of Chemical Resource Engineering, Beijing Advanced Innovation Center for Soft Matter Science and Engineering, Beijing University of Chemical Technology, Beijing 100029, PR China.
E-mail addresses: yangyusen@mail.buct.edu.cn (Y. Yang), zhangxin@mail.buct.edu.cn (X. Zhang), weimin@mail.buct.edu.cn (M. Wei).
[1] These authors contribute equally to this work.

https://doi.org/10.1016/j.apcatb.2024.123719
Received 9 November 2023; Received in revised form 20 December 2023; Accepted 7 January 2024
Available online 10 January 2024

prevailingly focuses on catalyst structure with specific type of active sites required for desired substrate adsorption and conversion [14–16]; whereas studies on the control of catalytic reaction parameters are often overlooked. In liquid-phase hydrogenation reactions, besides the electronic and geometric structure of catalyst active sites, the reaction solvent also has profound impact on the catalytic activity and selectivity. In addition to the well-known heat transfer, dissolution and heat sink effects, solvents would change surface chemistry *via* binding to active sites, stabilizing surface intermediates, or co-catalyzing proton-like transfer [17–21]. Previous studies have shown that the solvent can provide another route for tuning catalytic performance [22–24]; for instance, it has been reported that the hydrogenation rate of benzaldehyde to benzyl alcohol on a Pd/C catalyst differs by up to one order of magnitude in different solvents [25]. Although the possibility of solvent-induced reaction rate and product selectivity has been unveiled by these studies, the underlying factors governing reaction pathways in different solvents remain ambiguous. FAL represents a classic example for the challenge of product selectivity in liquid catalytic hydrogenation [26,27]; therefore, a systematic elucidation of solvent effects on FAL hydrogenation system is of great significance for an in-depth understanding of reaction mechanism as well as the development of biomass upgrading.

Herein, a heterogonous catalyst composed of fully-exposed Pt clusters immobilized on CoAl mixed metal oxides (denoted as Pt_n/CoAl-MMOs) was prepared using a two-step synthesis approach: structural topological transformation of layered double hydroxides (LDHs) precursor to CoAl-MMOs followed by a loading-reduction treatment. The as-obtained Pt_n/CoAl-MMOs catalyst exhibits a high product selectivity (> 90%) towards THFA, FA, 2-MF and FU when using ethanol, dioxane, isopropanol and *n*-hexane as solvent, respectively (Fig. 1). Interestingly, a facile selectivity switch can be achieved *via* tuning solvent within one catalytic reaction system, which is highly desirable for industrial applications. Electron microscopic and spectroscopic characterizations confirm the formation of fully-exposed Pt clusters, in which single-atomic-layer thick Pt clusters (~0.76 nm) are stabilized on CoAl-MMOs surface *via* Pt−Co and Pt−O bonds. Surface science studies (*in situ* FT-IR & TPSR-Mass) combined with theoretical calculations (DFT) disclose that the existence of solvent molecules would induce distinct adsorption configuration of FAL, thereby exerting a profound impact on hydrogenation pathway and product selectivity. In ethanol solvent, both C═C and C═O bonds undergo activation adsorption, leading to the complete hydrogenation of FAL to generate THFA. The dioxane solvent favors the activation adsorption of C═O group whilst suppresses the adsorption of furan ring, thereby facilitating the production of FA. The adsorption configuration of FAL in isopropanol solvent activates the aldehyde group and part of the furan ring, which facilitates the C−O cleavage and thus gives rise to the generation of 2-MF. In contrast, the *n*-hexane solvent accelerates the activation adsorption and breakage of the C−C bond and thus FU as the target product is obtained. The presence of solvents plays a decisive role on the adsorption behavior of FAL through modifying the solvent-catalyst and/or substrate-catalyst interaction, which eventually determines the hydrogenation pathway and final product.

Fig. 1. Selective hydrogenation reaction of FAL towards four individual products over Pt_n/CoAl-MMOs catalyst in the presence of various solvents.

2. Experimental Section

2.1. Chemicals and materials

Reagents, including $Co(NO_3)_2{\cdot}6\ H_2O$, $H_2PtCl_6{\cdot}6\ H_2O$, urea and $Al(NO_3)_3{\cdot}9\ H_2O$ were procured from Aladdin Chemical Reagent Company. Furfural (FAL), ethanol, dioxane, isopropanol and *n*-hexane were purchased from Sigma Aldrich.

2.2. Synthesis of catalysts

CoAl-LDHs precursor was synthesized through a urea decomposition method. Specifically, a solution was prepared by dissolving $Co(NO_3)_2{\cdot}6\ H_2O$ (0.05 M), urea (0.5 M) and $Al(NO_3)_3{\cdot}9\ H_2O$ (0.025 M) in 400 mL of purified water, followed by aging at 110 °C for 24 h. After centrifugation and fully washing, the resulting precipitate was dried overnight at 60 °C.

The Pt_n/CoAl-MMOs catalyst was prepared *via* a two-step synthesis route. In the first step, the CoAl-LDHs precursor underwent calcination (400 °C, air) for 4 h to yield CoAl-MMOs. In the second step, the Pt_n/CoAl-MMOs catalyst was synthesized through a loading-reduction treatment. 0.5 g of CoAl-MMOs were dispersed in 50 mL of water, followed by slow addition of 5.0 mL of H_2PtCl_4 aqueous solution (6.2 mmol L^{-1}) with vigorous stirring in a N_2 atmosphere for 16 h. The resulting powder was subsequently dried in a vacuum oven at 60 °C and then subjected to reduction in a 10% H_2/N_2 (v/v) atmosphere at 300 °C for 3 h. After being subjected to N_2 cooling until reaching ambient temperature, the Pt_n/CoAl-MMOs catalyst was obtained. The Pt_1/CoAl-MMOs sample was prepared using the same method, incorporating a precise volume of H_2PtCl_4 solution (1.7 mL).

2.3. Characterizations

The Rigaku XRD-6000 diffractometer was utilized for conducting the XRD measurements. The elemental composition of the samples was analyzed utilizing the ICP-AES (Shimadzu ICPS-7500). Sample morphology and structure were characterized using SEM with a Zeiss Supra 55 instrument, TEM with a JEOL JEM-2010 instrument, and AC-HAADF-STEM with a JEOL JEM-ARM200F instrument. The Pt L_3-edge *in situ* XAFS tests were conducted at beamline 1W1B of the Beijing Synchrotron Radiation Facility. In situ DRIFTS and FT-IR analyses were carried out using a customized *in situ* reaction cell, alongside an exquisitely sensitive MCT detector integrated into the Bruker TENSOR II infrared spectrometer. The temperature-programmed surface reaction (TPSR) measurements of FAL were conducted on a Micromeritics Autochem II 2920 device furnished with a mass spectrometry detector (MS). The Supplementary Information provides a comprehensive description of the detailed characterization methods.

2.4. Catalytic evaluations

A batch reaction was employed to evaluate the catalytic performance. To begin, FAL (0.25 mL), solvent (15 mL) and catalyst (50 mg) were added into a 50 mL stainless-steel autoclave. Subsequently, the reactor underwent thorough purging with H_2 (>99.999%) at 2.0 MPa for five cycles before being pressurized and sealed with H_2 at 3.0 MPa. The reaction commenced at 150 °C under continuous stirring at 800 rpm. Product identification and quantitative analysis were carried out using GC-MS (Agilent, 7890B GC/5977 A MS) and gas chromatograph spectrometer (Shimadzu GC-2014 C).

2.5. Computational method

Periodic DFT calculations with spin polarization were conducted employing the Vienna Ab initio Simulation Package (VASP 5.4.1). The projector augmented wave approach was utilized to describe the core electrons. The Kohn-Sham equations were successfully solved employing the Perdew-Burke-Ernzerhoff functional within the generalized gradient approximation (GGA). The inclusion of Grimme's DFT-D3 approach was implemented to consider the influence of van der Waals forces. The energies and residual forces were brought to a convergence threshold of 10^{-4} eV and 0.01 eV $Å^{-1}$, respectively. The transition states were obtained utilizing the Dimer method. The AIMD simulations were carried out at temperatures of 443.15, 393.15, 453.15 and 433.15 K for (a) ethanol, (b) dioxane, (c) isopropanol and (d) *n*-hexane in a canonical ensemble (NVT). The Supplementary Information provides a comprehensive description of the detailed computational methods.

3. Results and discussion

3.1. Structural characterizations of Pt_n/CoAl-MMOs

The XRD pattern of CoAl-layered double hydroxides (CoAl-LDHs) precursor (Fig. S1) shows characteristic reflections at 2θ 11.9° (003), 23.8° (006) and 34.8° (012), which are attributed to a typical LDHs phase [28]. SEM image illustrates a nanosheet-like morphology with a uniform lateral particle size of 2–3 μm (Fig. S2). The subsequent calcination process (air, 400 °C) triggers a structural topotactic transformation from LDHs to mixed metal oxides (CoAl-MMOs), whose XRD pattern displays a cubic Co_3O_4 phase (PDF#42–1467) without the presence of crystalline Al_2O_3 (*e.g.*, an amorphous phase) [29] (Fig. S1). Afterwards, Pt_n/CoAl-MMOs sample was obtained by loading-reduction method to introduce Pt clusters (loading content: 1.2 *wt.*%) onto the surface of CoAl-MMOs. No reflection of Pt (PDF#04–0802) is observed on Pt_n/CoAl-MMOs (Fig. S1), due to a high dispersion of platinum

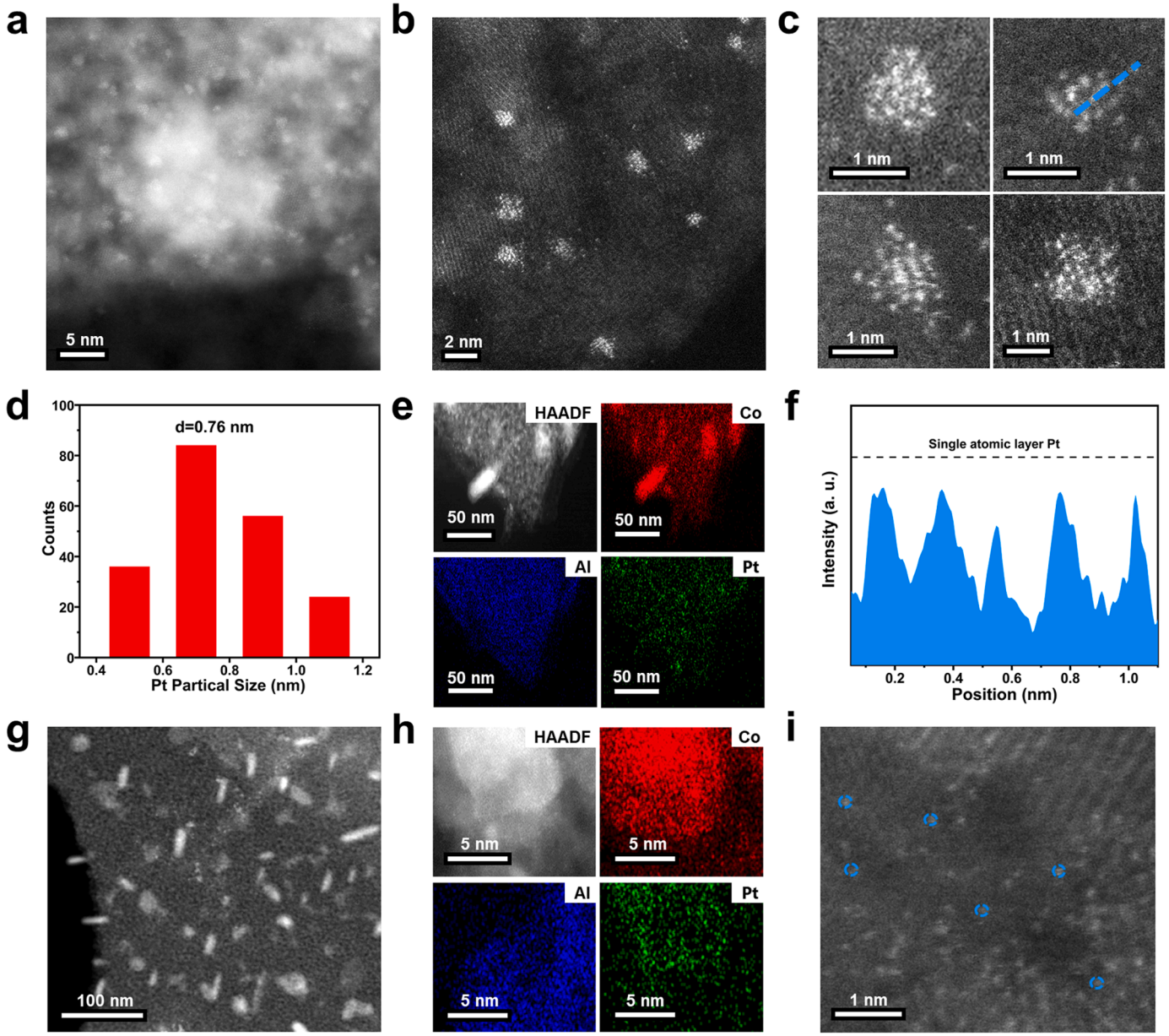

Fig. 2. Electron micrology studies on Pt_n/CoAl-MMOs and Pt_1/CoAl-MMOs samples. (a–c) AC-HAADF-STEM images of Pt_n/CoAl-MMOs sample. (d) Size distribution of Pt clusters. (e) STEM-EDS elemental mapping of Pt_n/CoAl-MMOs. (f) Line profile extracted along the blue dashed line in (c) demonstrates the single-atomic-layer thickness of Pt clusters. (g) STEM image, (h) STEM-EDS elemental mapping and (i) AC-HAADF-STEM image of Pt_1/CoAl-MMOs sample.

species that cannot be detected by XRD analysis [30]. SEM image (Fig. S2) illustrates a plate-like morphology of Pt_n/CoAl-MMOs sample inheriting from LDHs precursor; high-resolution transmission electron microscope (HR-TEM) image displays a lattice spacing of 0.466 nm, indicating the presence of the Co_3O_4(111) plane [31] (Fig. S3).

Aberration-correction high-angle annular dark-field scanning transmission electron microscopy (AC-HAADF-STEM) combined with energy-dispersive spectroscopy (EDS) was employed for further studying the atomic-scale structure of Pt_n/CoAl-MMOs sample. As shown in Fig. 2a–d, sub-nanometer Pt clusters (~0.76 nm) composed of several Pt atoms are clearly distinguished from the CoAl-MMOs matrix based on variations in brightness. EDS elemental mapping of Pt_n/CoAl-MMOs (Fig. 2e) illustrates a uniform distribution of Pt (green color) on the CoAl-MMOs substrate. These sub-nanometer Pt clusters displayed in Fig. 2f are characterized by a single-atomic-layer thickness, indicating that a maximum dispersion and full exposure of all Pt atoms are obtained without Pt−Pt overlay in the thickness direction. In addition, CO titration measurement (Table S1) gives a dispersion degree of 90.7% for Pt, providing further confirmation that the Pt clusters are predominantly fully-exposed on the CoAl-MMOs support. For reference, the Pt single-atom sample (Pt_1/CoAl-MMOs) is also prepared with Pt loading of 0.4%, whose STEM images (Fig. 2g–i) show several individual Pt atoms (highlighted by the blue circles) on the support surface without observation of Pt clusters or nanoparticles.

X-ray photoelectron spectroscopy (XPS) combined with *in situ* CO-diffuse reflectance infrared fourier transform spectroscopy (DRIFTS) was employed to investigate the surface chemical states of Pt species on Pt_1/CoAl-MMOs and Pt_n/CoAl-MMOs samples. As shown in Fig. 3a, the Pt 4*d* binding energy of Pt_n/CoAl-MMOs shifts to a lower value relative to Pt_1/CoAl-MMOs, which indicates an increased electronic density of the former sample. CO adsorption on CoAl-MMOs support is quite weak to be detected at room temperature (Fig. 3b). The Pt_1/CoAl-MMOs sample exhibits a weak peak at ~2087 cm^{-1}, attributed to the presence of linearly bonded CO at the isolated Pt site in an on-top configuration [32]. In contrast, the primary band at 2046 cm^{-1} over Pt_n/CoAl-MMOs is attributed to the bridge-adsorbed CO on Pt clusters [33]. X-ray absorption near edge structure (XANES) was employed to further confirm the local structure of Pt species. The normalized Pt L_3-edge XANES spectra of these two samples (Fig. 3c) show the white-line intensity located between the Pt foil and PtO_2 reference, suggesting that the Pt atom valence is situated between Pt^0 and Pt^{4+}. The Pt_1/CoAl-MMOs sample displays a higher energy of absorption edge than Pt_n/CoAl-MMOs, indicating a higher oxidation state in the former case. Moreover, in the EXAFS spectra of R-space (Fig. 3d), no typical peak corresponding to the Pt−Pt path contribution is detected for the Pt_1/CoAl-MMOs sample. In the case of Pt_n/CoAl-MMOs sample, one main peak at ~2.1 Å and two relatively weaker ones at ~1.5 and ~2.8 Å are observed, which are associated with the Pt−Co, Pt−O and Pt−Pt coordination, respectively. The Wavelet transform (WT) analysis of PtO_2 and Pt foil reveals the intensity at ~3 and ~7 $Å^{-1}$ attributed to Pt–O and Pt–Pt contribution, respectively (Fig. S4). In the contour plots of Pt_1/CoAl-MMOs, a main lobe at ~5 $Å^{-1}$ is assigned to the contribution of Pt−O and Pt−Co (Fig. 3e). For the sample of Pt_n/CoAl-MMOs (Fig. 3f), besides the same Pt−O and Pt−Co contribution mentioned above, an additional signal at ~6 $Å^{-1}$ (Pt−Pt coordination) signifies the occurrence of Pt aggregation, which agrees well with the results of HAADF-STEM.

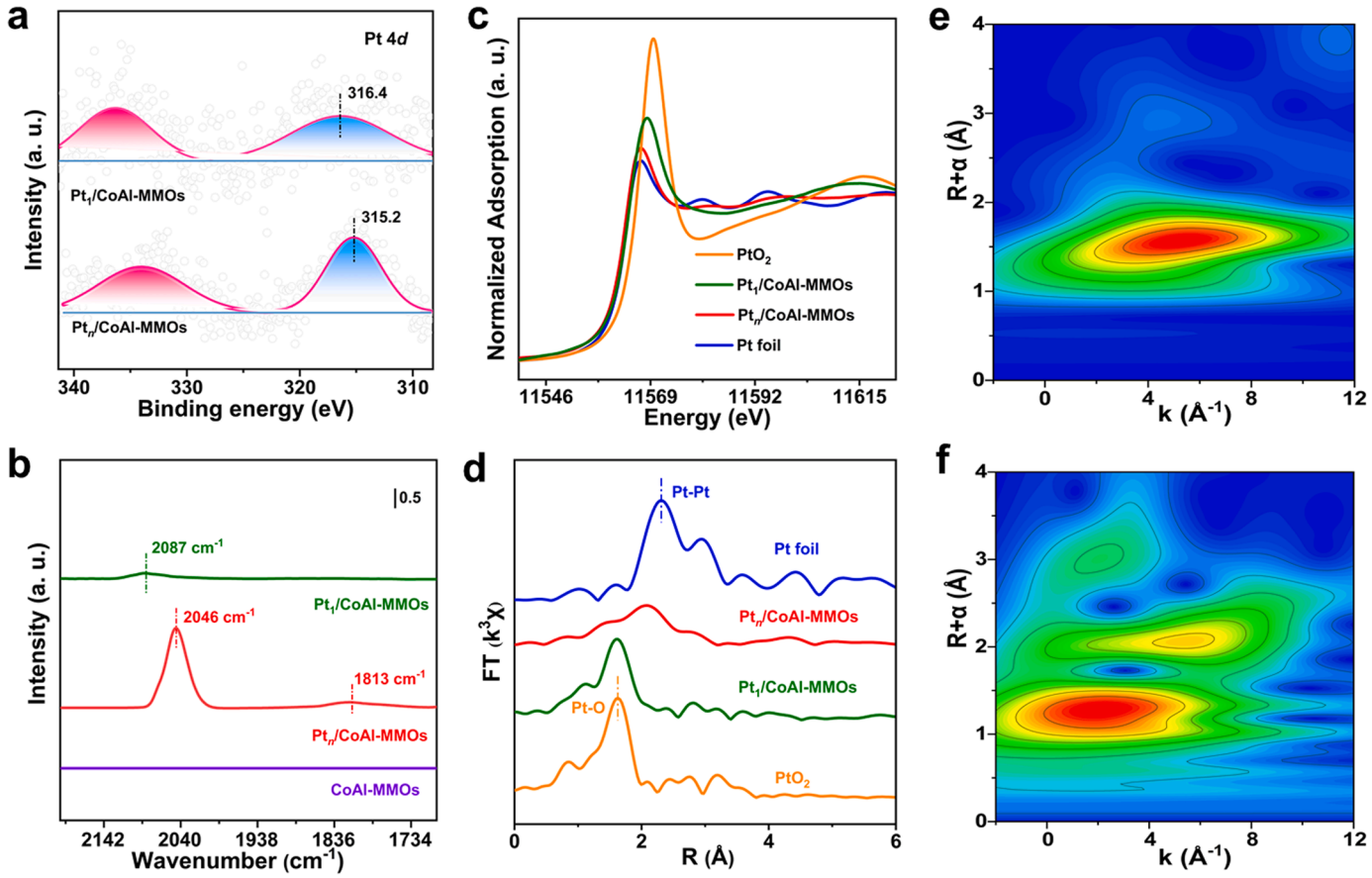

Fig. 3. Fine-structure characterizations of Pt_n/CoAl-MMOs and Pt_1/CoAl-MMOs samples. (a) XPS spectra of Pt *4d* for Pt_1/CoAl-MMOs and Pt_n/CoAl-MMOs. (b) In situ CO DRIFTS spectra for CoAl-MMOs, Pt_1/CoAl-MMOs and Pt_n/CoAl-MMOs. (c) XANES spectra and (d) Fourier transform (FT) at the Pt L_3-edge of Pt_1/CoAl-MMOs, Pt_n/CoAl-MMOs, PtO_2 and Pt foil. Wavelet transformation of (e) Pt_1/CoAl-MMOs and (f) Pt_n/CoAl-MMOs, respectively.

3.2. Catalytic evaluations towards selective hydrogenation of FAL

The reaction network of FAL hydrogenation contains three main routes (Fig. S5). In Route I, the aldehyde group undergoes hydrogenation to alcoholic group (FA), followed by hydrogenation of two C═C bonds in furan ring to generate THFA. In Route II, FAL is hydrogenated to FA as an intermediate product, and then FA experiences hydrogenolysis to produce 2-MF. In Route III, the aldehyde group in FAL is eliminated first to yield FU, followed by the hydrogenation of FU to obtain tetrahydrofuran (THF). Biomass upgrade reactions are normally conducted in a solvent due to the highly oxygenated nature of the feedstock [34]. The solvent effects in FAL hydrogenation reaction are examined herein with nonpolar solvent (*n*-hexane) and polar solvents (*i.e.*, ethanol, dioxane and isopropanol). The catalytic conversion of FAL has been screened over CoAl-MMOs, Pt_1/CoAl-MMOs and Pt_n/CoAl-MMOs samples at 150 °C and 3 MPa of H_2, using ethanol, dioxane, isopropanol and *n*-hexane as solvent, respectively (Table 1). The pristine CoAl-MMOs support gives a poor catalytic activity in these four solvents. The Pt_1/CoAl-MMOs sample shows a 100% FAL conversion in these four solvents, but the selectivity of specific product is low (< 60%). In contrast, the Pt_n/CoAl-MMOs catalyst not only displays a high hydrogenation activity (conversion: 100%), but also exhibits distinct product distributions in these four solvents. Under the identical reaction conditions, 80.2% selectivity towards THFA (in ethanol), 89.9% selectivity to FA (in dioxane), 84.9% selectivity towards 2-MF (in isopropanol) and 80.0% selectivity to FU (in *n*-hexane) are obtained, respectively, which verifies the decisive role of solvent in determining the product selectivity. Encouraged by these results, the reaction kinetic curves of FAL hydrogenation over Pt_n/CoAl-MMOs catalyst were further investigated in ethanol, dioxane, isopropanol and *n*-hexane, respectively. Interestingly, as shown in Fig. S6, FA is detected in all these four reaction systems. In the case of dioxane solvent, the amount of FA is cumulative to the maximum at 1.5 h and then remains stable within 1.5 − 3 h as the final product. In contrast, when using ethanol, isopropanol and *n*-hexane as the solvent, FA increases first and then declines in yield with a volcanic type concentration distribution curve, indicating that FA is a crucial intermediate during the hydrogenation reaction of FAL.

A detailed investigation on FAL hydrogenation was performed over the Pt_n/CoAl-MMOs catalyst in these four individual solvents (ethanol, dioxane, isopropanol and *n*-hexane), and Fig. S7— **10** showed the relationship between catalytic performance and reaction conditions (reaction temperature, hydrogen pressure and reaction time). Meanwhile, the temperature-programmed surface reaction (TPSR) measurements were conducted to identify the reaction pathways of FAL hydrogenation over Pt_n/CoAl-MMOs in these four solvents. In ethanol, the THFA selectivity initially enhances and then decreases as the reaction temperature rises and reaches the highest value (91.4%) at 170 °C (Fig. S7); an increase of H_2 pressure to 3 MPa leads to a linearly increased FAL conversion to 100%. TPSR results (Fig. S11a) show a desorption peak at ~135 °C in ethanol, which is attributed to the full hydrogenation of FAL (hydrogenation of both furan ring and C═O). In the case of dioxane, under the mild reaction conditions (120 °C, 0.8 MPa), a 97.7% yield of FA is obtained (Fig. S8). An FA desorption signal is observed at a low-temperature (~106 °C) in TPSR curve (Fig. S11b), which is due to the hydrogenation of C═O group in FAL. This indicates the desorption of intermediate (FA) from the catalyst surface is rather facile, consistent with the results of catalytic evaluations. In isopropanol, the optimal reaction conditions are selected as a reaction temperature of 180 °C and a hydrogen pressure of 2 MPa, giving rise to a 2-MF yield of 92.1% (Fig. S9). As verified by TPSR (Fig. S11c), a desorption signal assigned to 2-MF is detected at ~110 °C, indicating FAL undergoes hydrodeoxygenation reaction over Pt_n/CoAl-MMOs catalyst. Finally, in the case of *n*-hexane, the FU selectivity decreases as the reaction temperature exceeds 160 °C; and the maximum yield of FU (90.8%) is achieved at 160 °C with 4 MPa of hydrogen pressure (Fig. S10). As depicted in Fig. S11d, FU desorption peak is observed at ~142 °C resulting from the decarbonylation reaction of FAL. Based on the above consequence, the optimized catalytic performances of Pt_n/CoAl-MMOs catalyst towards the hydrogenation reaction of FAL in these four solvents are summarized in Table 2, all of which display satisfactory yields of four individual target products (> 90%). In addition, the recycling tests for Pt_n/CoAl-MMOs catalyst were performed in these four solvents; the yield of corresponding products gives a slight decrease within 4% after five recycles (Fig. S12). The XRD, SEM and AC-HAADF-STEM results of the used catalyst do not show obvious change in comparison with the fresh one (Fig. S13, S14), and only a slight loss (0.1%) in the Pt content is detected (Table S2), demonstrating a satisfactory stability and reusability of the Pt_n/CoAl-MMOs catalyst.

To investigate the possibility of solvent-dependent product selectivity over other metallic catalysts, Pd/CoAl-MMOs and Ni/CoAl-MMOs were prepared for the catalytic evaluations in ethanol, dioxane, isopropanol and *n*-hexane, respectively (Fig. S15). The Ni/CoAl-MMOs sample shows unsatisfactory catalytic activity in these four solvents; whilst the Pd/CoAl-MMOs sample displays a high hydrogenation activity (100% FAL conversion). Similar to the case of Pt_n/CoAl-MMOs catalyst, solvent imposes a great influence on the product distribution for both Pd/CoAl-MMOs and Ni/CoAl-MMOs catalysts; however, more pronounced side reactions occur on Ni/CoAl-MMOs. The FAL hydrogenation reaction on Pt_n/CoAl-MMOs was further examined in various solvents (Fig. S16). A high conversion (> 98.8%) of FAL is achieved in all solvents listed in Fig. S16, confirming the high catalytic activity of Pt_n/CoAl-MMOs for the hydrogenation of FAL. THFA is the main product in primary alcohol solvents; moreover, the yield of THFA exhibits a volcano-shaped trend with the increase of carbon number from 1 to 4,

Table 1
FAL Hydrogenation over various catalyst samples in the four individual solvents[a].

Catalyst	Solvent	Conversion (%)	Selectivity (%)					Yield of dominant product (%)
			FA	THFA	2-MF	FU	Others[b]	
Pt_n/CoAl-MMOs	ethanol	100	2.1	80.2	15.2	0	2.5	80.2
	dioxane	100	89.9	1.7	8.4	0	0	89.9
	isopropanol	100	4.1	5.2	84.9	5.7	0.1	84.9
	n-hexane	100	3.5	2.3	14.0	80.0	0.2	80.0
Pt_1/CoAl-MMOs	ethanol	100	7.6	28.7	47.9	0	15.8	47.9
	dioxane	100	53.5	3.1	22.0	19.9	1.5	53.5
	isopropanol	100	5.0	14.6	59.5	0.3	20.6	59.5
	n-hexane	100	11.2	7.8	29.7	51.3	0	51.3
CoAl-MMOs	ethanol	24.9	87.4	2.0	10.0	0.1	0.5	-
	dioxane	23.3	96.8	1.5	0.9	0	0.8	22.6
	isopropanol	26.4	68.2	7.9	23.2	0.2	0.5	-
	n-hexane	18.6	90.8	2.4	5.5	1.2	0.1	-

[a] Reaction conditions: 0.25 mL of FAL, 50 mg of catalyst, 3 MPa of H_2, 150 °C, 180 min, a stirring rate of 800 rpm. All results give a carbon balance above 95%.
[b] Other products mainly include pentanediol, methyl tetrahydrofuran (MTHF) and THF.

Table 2
FAL Hydrogenation over Pt_n/CoAl-MMOs under optimized reaction conditions in various solvents[a].

Solvent	Reaction conditions	Conversion (%)	Selectivity (%)					Yield of dominant product (%)
			FA	THFA	2-MF	FU	Others[b]	
ethanol	170 °C, 3 MPa of H_2, 3 h	100	0	91.4	0.6	0	8.0	91.4
dioxane	120 °C, 0.8 MPa of H_2, 5 h	99.0	98.7	0.8	0.2	0	0.3	97.7
isopropanol	180 °C, 2 MPa of H_2, 4 h	100	0.7	5.2	92.1	0	2.0	92.1
n-hexane	160 °C, 4 MPa of H_2, 4 h	100	2.2	4.8	2.0	90.8	0.2	90.8

[a] All results give a carbon balance above 95%
[b] Other products mainly include pentanediol, methyl tetrahydrofuran (MTHF) and THF.

and the highest yield is obtained in ethanol solvent. The main product in secondary alcohol solvents is 2-MF, whose selectivity decreases with the increase of carbon number due to the formation of by-products such as MTHF. In hydrocarbon solvents (*n*-hexane, octane and dodecane), FAL converts to furan over Pt_n/CoAl-MMOs. In addition, the catalytic performance of Pt-based catalysts on other supports was investigated in the FAL hydrogenation reaction using ethanol, dioxane, isopropanol and *n*-hexane as solvents (Fig. S17). Both the catalyst support and solvent greatly influence the distribution of products on Pt/SiO_2 or Pt/Al_2O_3 sample; however, in comparison with Pt_n/CoAl-MMOs, they do not show significant selectivity control towards a single product. The unique fine structure of the Pt_n/CoAl-MMOs catalyst, in conjunction with solvent effects, constitutes the fundamental rationale for product-switching outcomes.

3.3. Studies on structure-selectivity correlation

The adsorption configuration of substrate exerts a significant effect on hydrogenation reaction pathway and selectivity; therefore, *in situ* FT-IR measurements combined with theoretical calculations were employed to investigate the activation adsorption of FAL on Pt_n/CoAl-MMOs surface in the presence of four individual solvents. As a reference, four bands located at 1156, 1279, 1570 and 1686 cm^{-1} are found for the gas phase FAL (Fig. 4a), corresponding to ν(O2 −C5), ν(C2 −O2), ν(C═C) and ν(C1 =O1), respectively [35]. A noticeable red-shift of ν(C1 =O1) is observed from gas phase FAL to 1667 cm^{-1} (in dioxane), 1661 cm^{-1} (in *n*-hexane), 1657 cm^{-1} (in isopropanol) and then to 1623 cm^{-1} (in ethanol), which indicates a significant enhancement in the adsorption activation of the C1 =O1 group on the catalyst surface in the presence of solvent. The disappearance of corresponding IR signals has been observed upon chemical adsorption of certain group on the catalyst surface, owing to the constrained state of bridge/-multicoordinated adsorption [36]. As for FAL adsorption with ethanol (Fig. 4a), the absence of peaks for ν(C═C), ν(C2 −O2) and ν(O2 −C5) indicates a strong chemisorption of the furan ring on the catalyst surface. DFT calculations show that FAL molecule adopts a flat adsorption configuration in ethanol solvent, due to the very weak interaction between ethanol and Pt_n cluster (Fig. 4e and Figs. S18−**S23**). The adsorption energy of ethanol on plane, edge and corner site of Pt_n gives the following order: $E_{ads,plane}$ (−1.17 eV) > $E_{ads,edge}$ (−1.23 eV) > $E_{ads,corner}$ (−1.39 eV). The adsorption of ethanol molecule at the plane site of Pt_n is the weakest, resulting in a successful competitive adsorption of FAL molecule at this site. The optimal adsorption configuration of FAL is shown in **Fig. 19**d, in which both the C1 =O1 group and furan rings bind to the surface of Pt_n cluster, exhibiting an adsorption energy of − 6.09 eV. Moreover, the bond length of C1 =O1, C2 =C3 and C4 =C5 extend to 1.381, 1.415 and 1.522 Å, respectively (Table S3), relative to their gas phase values (1.229, 1.382 and 1.373 Å), indicating the activation adsorption of all unsaturated groups in FAL molecule onto Pt_n surface.

Whereas, for the FAL adsorption with dioxane solvent (Fig. 4b), in addition to the ν(C1 =O1) at 1667 cm^{-1}, the bands of ν(C═C), ν(C2 −O2) and ν(O2 −C5) are observed at 1571, 1280 and 1155 cm^{-1}, respectively, which implies the free-state of furan ring without activation adsorption. This is ascribed to the strong adsorption of dioxane molecule at the plane (−2.17 eV), edge (−2.46 eV) and corner (−2.34 eV) positions of Pt_n, which occupies a large portion of the surface active sites (Fig. S24). In this case, the C1 =O1 group in FAL experiences activation adsorption at the plane site of Pt_n ($E_{ads,plane}$(FAL)= −1.25 eV) with a vertical configuration (Fig. 4f and Fig. S24). The O1 atom of aldehyde group is activated, accompanied with the electron transfer from Pt to O1.

In the case of FAL with isopropanol (Fig. 4c), the band of ν(O2 −C5) is absent, indicative of the activation adsorption of O2 −C5 group. DFT calculations show that isopropanol molecule exhibits a medium interaction with catalyst, displaying adsorption energies of − 1.75, − 1.36 and − 1.37 eV at the plane, edge and corner sites of Pt_n, respectively (Fig. S25). This results in the preferential adsorption of FAL at the edge/corner site of Pt_n (E_{ads}: −2.69 eV), in which FAL molecule undergoes C1 =O1 double adsorption with an upright configuration of furan ring. The charge density difference results in electron transfer from Pt_n to the C1 =O1 group, leading to the activation of aldehyde group in FAL. Moreover, the bond length of C1 =O1 in aldehyde group is stretched to 1.492 Å after adsorption, significantly longer than that of the gas-phase FAL molecule (1.229 Å) and those in *n*-hexane (1.328 Å) and ethanol (1.381 Å) solvent (Fig. S18 and Table S3). This indicates a notable enhancement in the activation adsorption of C1 =O1 bond on Pt_n surface in the presence of isopropanol. Additionally, the hydrogen bond between isopropanol solvent and the O atom in furan ring ($E_{interaction}$= 0.16 eV) have a weak effect on the adsorption of FAL (Table S4).

For FAL with *n*-hexane (Fig. 4d), both ν(C═C) and ν(C2 −O2) are detected whilst ν(O2 −C5) band disappears, indicating an activation adsorption of partial furan ring on the catalyst surface. According to the DFT calculations, the adsorption energy of *n*-hexane molecule shows the following sequence: $E_{ads,corner}$(−0.56 eV) > $E_{ads,edge}$(−1.45 eV) > $E_{ads,plane}$(−1.52 eV) (Fig. S26). The preferential occupancy of the plane and edge sites by solvent results in the activation adsorption of FAL at the corner site of Pt_n with an adsorption energy of − 3.92 eV, where the C1 =O1 group binds to adjacent Pt−Pt sites whilst the furan ring exhibits a weak and tilted physical adsorption on the Pt_n surface (Fig. S26d). The bond length of C1–C2 is stretched to 1.489 Å, much longer than the gas-phase FAL molecule (1.448 Å), indicating a specific activation of the C1–C2 bond on Pt_n (Table S3). The analysis of charge density difference illustrates that electron transfers from Pt_n to C1 =O1 group and the C1 −C2 bond connected with aldehyde group, which further confirms the activation adsorption of aldehyde group and a portion of furan ring in FAL (Fig. S26f). As for FAL adsorption on Pt_n/CoAl-MMOs surface in the absence of solvent, a red-shift of ν(C1 =O1) is observed and the two bands of ν(C═C) and ν(C2 −O2) are negligible (Fig. S27), indicating both C═O bond and furan ring undergo chemisorption on the surface of catalyst (flat adsorption configuration). As shown in Fig. S28, in the absence of solvent, the adsorption energies of the four types of FAL adsorption configurations on Pt_n give the following order: $E_{ads\ flat}$ (–6.09 eV) < $E_{ads,\ tilted}$ (−3.92 eV) < $E_{ads,\ C═O\ double\ adsorption}$ (–2.69 eV) < $E_{ads,\ vertical}$ (–1.25 eV), further confirming that the flat adsorption is the optimal adsorption configuration. In addition, we assessed the interactions between adsorbed FAL and solvent molecule on the catalyst surface, respectively. The results of DFT calculations show

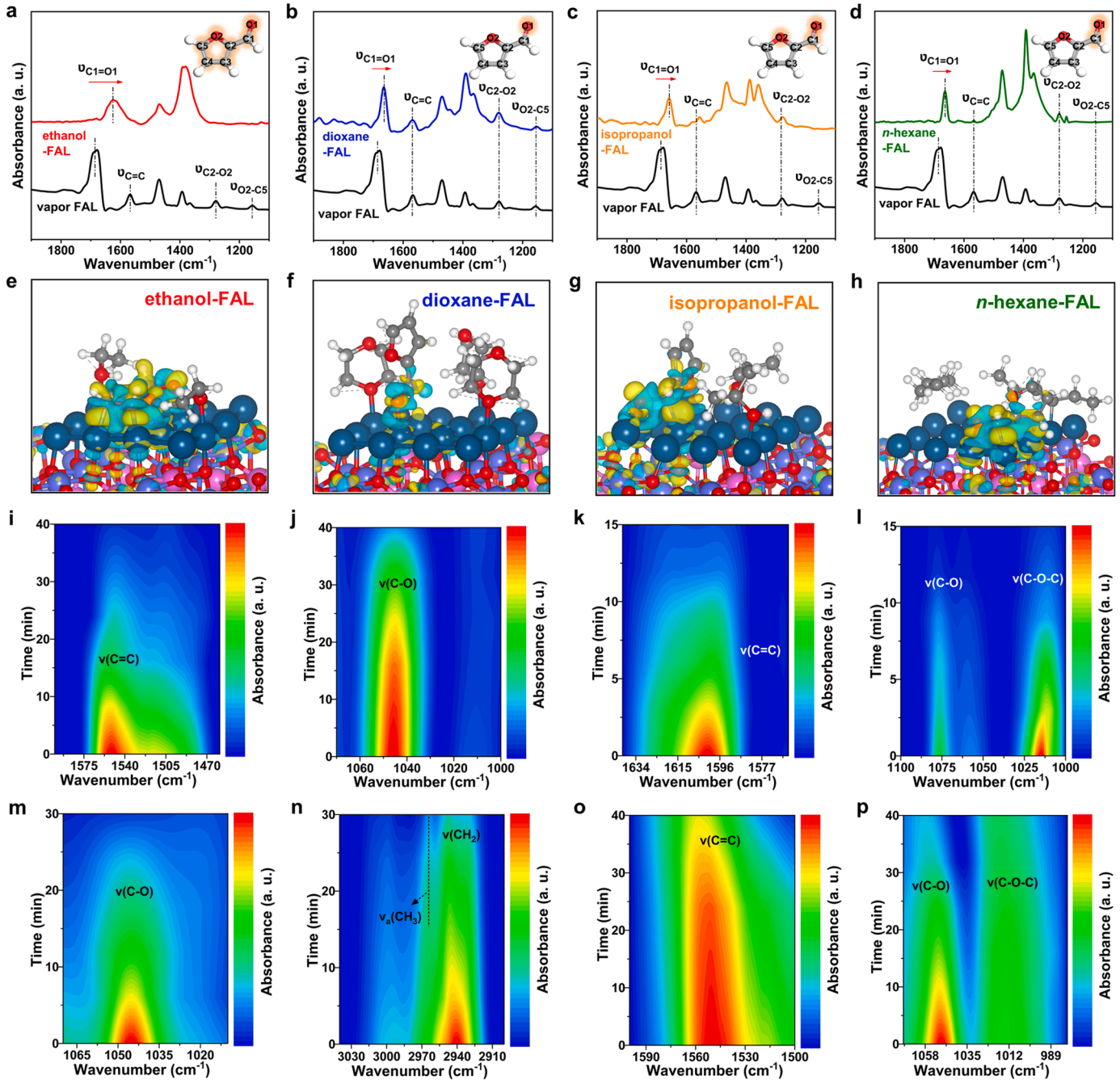

Fig. 4. Studies on the solvent effect in the presence of Pt_n/CoAl-MMOs catalyst. In situ FT-IR spectra of FAL adsorption on Pt_n/CoAl-MMOs sample acquired within 1900 – 1100 cm^{-1} through flowing solvents (a) ethanol, (b) dioxane, (c) isopropanol and (d) *n*-hexane for 15 min and then FAL for 15 min, followed by He flushing for 15 min. Charge density difference for FAL adsorption with (e) ethanol, (f) dioxane, (g) isopropanol and (h) *n*-hexane on the surface of Pt_n/CoAl-MMOs. The pink, blue, red, white and purple balls denote Al, Pt, O, H and Co atoms, respectively. Cyan and yellow contours represent the accumulation and depletion of electrons. In situ FT-IR spectra of the hydrogenation progress of FA over Pt_n/CoAl-MMOs sample through flowing (i,j) ethanol, (k,l) dioxane, (m,n) isopropanol and (o,p) *n*-hexane solvents, with H_2 as a reaction gas.

that the intermolecular distance between FAL and solvent molecule exceeds 2.0 Å (Fig. S16). The adsorption energy of FAL exhibits a slight increase upon solvent addition (Table S4), indicating a relatively weak interaction between FAL and solvent. Therefore, the impact of substrate-solvent interaction on competitive adsorption and reaction selectivity is minimal or even negligible.

Since FA is the key intermediate in FAL hydrogenation reaction, *in situ* FT-IR spectroscopy was employed to study the dynamic catalytic reaction process of FA on Pt_n/CoAl-MMOs with the presence of individual solvent (ethanol, dioxane, isopropanol and *n*-hexane). The FT-IR spectra of gaseous FA exhibits three characteristic bands located at 1015, 1078 and 1600 cm^{-1}, corresponding to ν_s(C−O−C), ν(C−O) and ν(C═C), respectively (Fig. S29) [36,37]. In the case of FA with ethanol system (Fig. 4i,j), both the C−O (1046 cm^{-1}) and C═C (1541 cm^{-1}) bands show a red-shift, implying the activation adsorption of both C−OH and furan ring on the catalyst surface. Afterwards, hydrogen is introduced into the reactor, and the ν(C═C) band rapidly shrinks within 0 – 40 min whilst the band of ν(C−O) exhibits a slow decline. This manifests the hydrogenation of C═C bond in furan ring, leading to the formation of THFA. DFT calculations results indicate that FA molecule

exhibits a flat adsorption configuration on Pt cluster in ethanol solvent (E_{ads}= −5.11 eV), and the analysis of charge density difference shows a strong electron interaction between the C═C bond in furan ring and the catalyst surface (Fig. S30). These findings suggest that FA in ethanol solvent is inclined to undergo hydrogenation, resulting in the formation of THFA. In contrast, for the FA with dioxane system (Fig. 4k,l), a slight red-shift of C−O band is found (1075 cm^{-1}) relative to gaseous FA (Fig. S29), and the adsorption energy of FA on the catalyst surface (E_{ads}= −1.75 eV) is less than that of dioxane solvent (E_{ads}= −2.17 eV), indicating FA molecule is more likely to desorption from the catalyst surface than solvent molecule. This is indeed the case: upon a continuous hydrogen inflowing, both C−O and C═C signals progressively decline and completely vanish within 15 min, indicating the desorption of FA molecule from catalyst surface rather than further reaction.

As for FA with isopropanol solvent (Fig. 4m,n), under on-stream hydrogenation conditions, the band of ν(C−O) (1048 cm^{-1}) rapidly diminishes accompanied by a rather slight decline of ν(C═C); whilst a new methyl-related band emerges at 2964 cm^{-1}. This verifies a significant C−O cleavage over Pt_n/CoAl-MMOs in isopropanol solvent, in accordance with the optimal selectivity toward 2-MF. Based on DFT calculations, it is observed that the bond length of C1–O1 in alcohol group is stretched to 1.505 Å for the adsorbed FA molecule, which is notably longer compared to that of gaseous FA molecule (1.428 Å) (Table S5). This finding confirms a significantly enhanced C–O cleavage facilitated by Pt_n/CoAl-MMOs in isopropanol solvent.

In the case of FA with *n*-hexane, the characteristic signal of C−O bond gives a red-shift to 1050 cm^{-1} relative to gaseous FA, which completely disappears after H_2 purging for 42 min; whilst the peak of ν(C═C) and ν_s(C−O−C) are still apparent (Fig. 4o,p). According to the catalytic reaction results, this indicates the scission of C1−C2 bond in FA to produce FU. DFT calculations show that the C1 −C2 bond length of FA in *n*-hexane solvent increases by 0.048 Å compared to gas-phase FA (Table S5). Furthermore, Bader charge analysis (Table S6) and charge density difference (Fig. S30) demonstrate a noticeable attenuation in electron density of the C1 −C2 bond in FA upon its adsorption on the Pt_n surface. This indicates that Pt atoms effectively boost the cleavage of C−C bond in the presence of *n*-hexane solvent, resulting in the formation of FU.

The computational energy profile and reaction mechanism (Fig. 5) of FAL hydrogenation on Pt_n/CoAl-MMOs in four solvents were studied *via* DFT calculations, with detailed intermediate structure for elementary steps shown in Fig. S31— **34**. In the case of FAL with ethanol solvent (Fig. 5a), the carbonyl O atom of FAL is hydrogenated to form F−CHOH intermediate, followed by a second hydrogenation step to generate FA intermediate, with energy barriers of 0.32 and 0.98 eV, respectively. Subsequently, the furan ring undergoes hydrogenation with energy barriers of 0.63, 0.25, 0.99 and 0.15 eV for C3, C4, C5 and C2 hydrogenation, respectively. The entire hydrogenation process of FAL to THFA is endothermic and the C4 hydrogenation is the rate-determining step. For FAL with dioxane solvent (Fig. 5b), the H atom adsorbed at Pt top site undergoes migration to O1 for the initial hydrogenation, generating hydroxyalkyl intermediate, followed by the second hydrogenation on C1

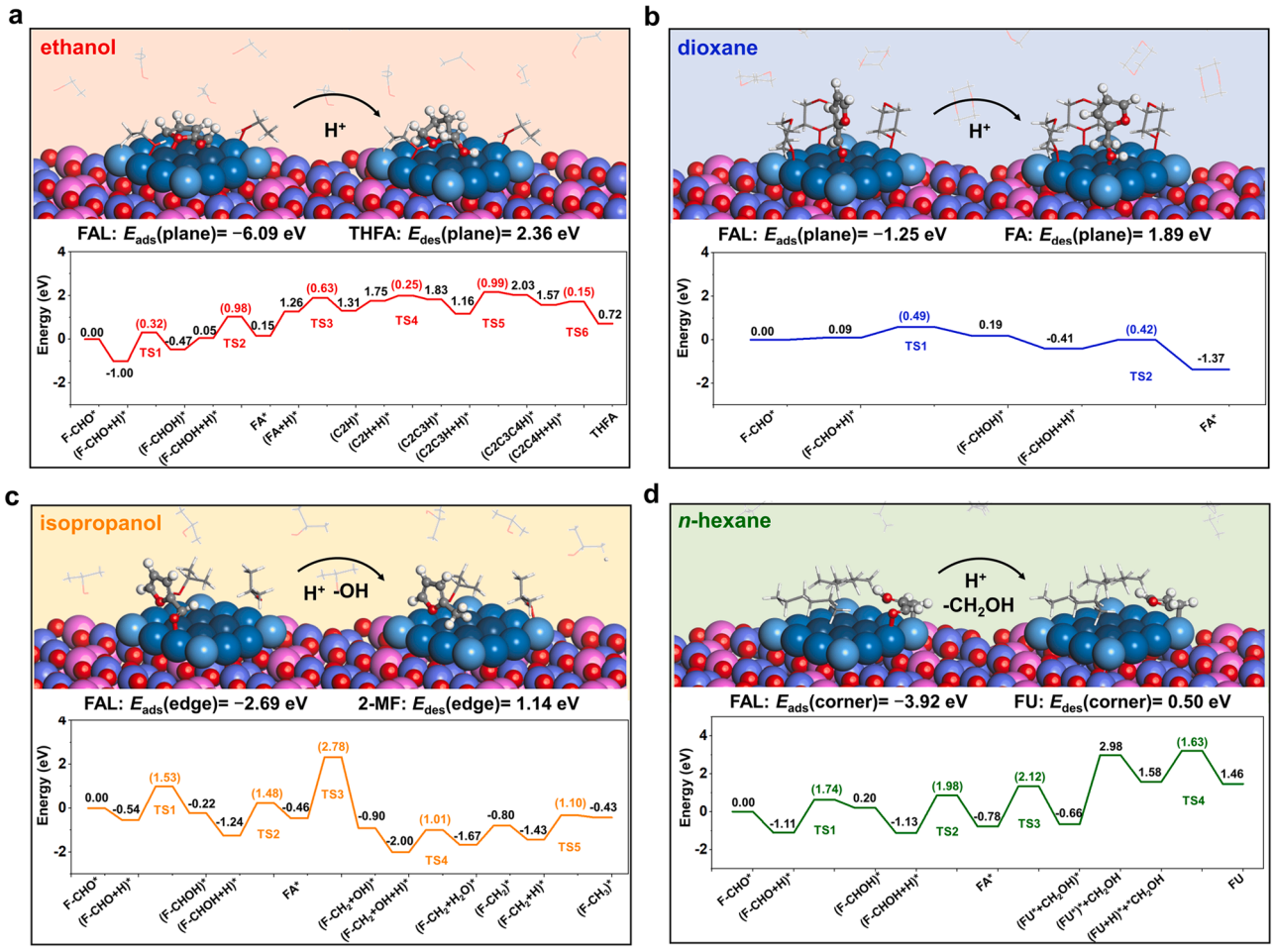

Fig. 5. Hydrogenation reaction of FAL on Pt_n/CoAl-MMOs in the presence of four individual solvents. Potential energy profiles and schematic illustration for the catalytic hydrogenation of adsorbed FAL on Pt_n/CoAl-MMOs covered with (a) two ethanol molecules; (b) three dioxane molecules; (c) two isopropanol molecules; (d) two *n*-hexane molecules.

to produce FA. The energy barriers of these two hydrogenation steps are 0.49 and 0.42 eV, respectively, with the initial hydrogenation step serving as the rate-determining process. In the presence of isopropanol solvent (Fig. 5c), the conversion of FAL to 2-MF encompasses three processes. Firstly, FAL undergoes a two-step hydrogenation to generate FA. Subsequently, the C−OH bond in F−CH_2 −OH breaks to form intermediates (F−CH_2 * and HO*) with an energy barrier of 2.78 eV, which represents the rate-determining step. Finally, products F−CH_3 (2-MF) and H_2O are obtained *via* hydrogenation of intermediates (F−CH_2 * and HO*), with energy barriers of 1.01 and 1.10 eV, respectively. In the case of FAL with *n*-hexane solvent (Fig. 5d), the inclined adsorption configuration of FAL promotes the carbonyl hydrogenation (1.74 and 1.98 eV) and then the cleavage of C−C bond (2.12 eV) between aldehyde and furan ring. Subsequently, the furan ring experiences hydrogenation to form FU with an energy barrier of 1.63 eV. The entire FAL hydrogenation process leading to FU is exothermic and the hydrogenation of furan ring is the rate-determining step. Among these four solvents, it is found that the reaction energy barrier of FAL to FA is the lowest (in dioxane solvent), which accords well with the experimental conditions where low temperature and pressure (120 °C, 0.8 MPa) are sufficient to promote the hydrogenation of FAL. Conversely, among the four reaction routes, the highest energy barrier is associated with the C−OH bond breakage in isopropanol solvent, which corresponds to the relatively harsh reaction conditions (180 °C, 2 MPa) of FAL conversion to 2-MF.

Solvent, as a crucial component of the catalytic system, can effectively modulate the product selectivity, and such regulatory effects stem from the solvent-catalyst and/or substrate-catalyst interaction. We have observed that the solvent and substrate compete for adsorption sites onto the Pt_n surface. The strength of the solvent-catalyst interaction (ethanol < *n*-hexane < isopropanol < dioxane) determines the adsorption configuration of FAL (changing from flat to vertical orientation), which ultimately dictates the hydrogenation pathway, key intermediate and final product. It is noteworthy that competitive adsorption is site-specific, which indicates that a reaction may occur exclusively at a particular site due to the occupation of other sites by substrate-independent species. However, the reaction activity cannot be directly correlated to the solvent-catalyst interaction, which is likely due to the intrinsic catalytic activity of the catalyst. The substrate-solvent competitive adsorption observed in this work may be quite general, particularly for biomass-derived compounds containing multiple functional groups that can simultaneously interact with specific surface sites.

4. Conclusion

In summary, we report a fully exposed Pt clusters immobilized on CoAl-MMOs catalyst (Pt_n/CoAl-MMOs), which exhibits a switchable product selectivity (> 90%) towards THFA, FA, 2-MF and FU when using ethanol, dioxane, isopropanol and *n*-hexane as solvent, respectively. Experimental and theoretical assessments unveil that the solvent-catalyst and substrate-catalyst interaction govern the adsorption configuration of FAL molecule, which ultimately determines the hydrogenation pathway and final product. This study provides an efficient product-switching strategy in one catalytic system, which offers an additional tool to improve the efficiency of catalytic processes *via* controlling the potential adsorption sites at liquid-solid interfaces.

CRediT authorship contribution statement

Zhao Shiquan: Investigation. **Liu Tianyong:** Investigation. **Li Feng:** Methodology. **Zhang Xin:** Investigation, Writing – review & editing. **Zhang Yuanjing:** Data curation, Formal analysis, Writing – original draft. **Hong Song:** Methodology. **Zheng Lirong:** Methodology. **Wang Lei:** Methodology. **Xu Enze:** Methodology. **Wei Min:** Conceptualization, Writing – review & editing. **Wang Si:** Investigation, Writing – original draft. **Yang Yusen:** Conceptualization, Writing – review & editing. **Hou Quandong:** Methodology.

Declaration of Competing Interest

We declare that we have no financial and personal relationships with other people or organizations that can inappropriately influence our work, there is no professional or other personal interest of any nature or kind in any product, service and company that could be construed as influencing the position presented in the manuscript entitled "**A switchable hydrogenation chemoselectivity of biomass platform compounds based on solvent regulation**".

Data Availability

Data will be made available on request.

Acknowledgements

This work was supported by the National Natural Science Foundation of China (22172006, 22173003, 22102006 and 22288102), and the National Key R&D Program of China (2021YFC2103500). The authors are thankful for the support of the BSRF (Beijing Synchrotron Radiation Facility) during the XAFS measurements at the beamline of 1W1B and 1W2B.

Appendix A. Supporting information

Supplementary data associated with this article can be found in the online version at doi:10.1016/j.apcatb.2024.123719.

References

[1] E.M. Rubin, Genomics of cellulosic biofuels, Nature 454 (2008) 841–845.
[2] L. Lin, X. Han, B. Han, S. Yang, Emerging heterogeneous catalysts for biomass conversion: studies of the reaction mechanism, Chem. Soc. Rev. 50 (2021) 11270–11292.
[3] R. Zheng, Z. Liu, Y. Wang, Z. Xie, M. He, The future of green energy and chemicals: rational design of catalysis routes, Joule 6 (2022) 1148–1159.
[4] Y. Román-Leshkov, C. Barrett, Z. Liu, J.A. Dumesic, Production of dimethylfuran for liquid fuels from biomass-derived carbohydrates, Nature 447 (2007) 982–985.
[5] S. Li, M. Dong, J. Yang, X. Cheng, X. Shen, S. Liu, Z. Wang, X. Gong, H. Liu, B. Han, **Selective hydrogenation of 5-(hydroxymethyl)furfural to 5-methylfurfural over single atomic metals anchored on Nb_2O_5**, Nat. Commun. 12 (2021) 584.
[6] C. Wang, L. Wang, J. Zhang, H. Wang, J.P. Lewis, F.S. Xiao, Product selectivity controlled by zeolite crystals in biomass hydrogenation over a palladium catalyst, J. Am. Chem. Soc. 138 (2016) 7880–7883.
[7] S. Shi, P. Yang, C. Dun, W. Zheng, J.J. Urban, D.G. Vlachos, **Selective hydrogenation *via* precise hydrogen bond interactions on catalytic scaffolds**, Nat. Commun. 14 (2023) 429.
[8] A. Jaswal, P.P. Singh, T. Mondal, Furfural – a versatile, biomass-derived platform chemical for the production of renewable chemicals, Green. Chem. 24 (2022) 510.
[9] W. Lin, Y. Zhang, Z. Ma, Z. Sun, X. Liu, C.C. Xu, R. Nie, **Synergy between Ni_3Sn_2 alloy and Lewis acidic ReO_x enables selectivity control of furfural hydrogenation to cyclopentanone**, Appl. Catal. B 340 (2024) 123191.
[10] X. Meng, Y. Yang, L. Chen, M. Xu, X. Zhang, M. Wei, **A control over hydrogenation selectivity of furfural *via* tuning exposed facet of Ni catalysts**, ACS Catal. 9 (2019) 4226–4235.
[11] Q. Yang, D. Gao, C. Li, S. Wang, X. Hu, G. Zheng, G. Chen, Highly dispersed Pt on partial deligandation of Ce-MOFs for furfural selective hydrogenation, Appl. Catal. B 328 (2023) 122458.
[12] Z. Jin, X. Yi, L. Wang, S. Xu, C. Wang, Q. Wu, L. Wang, A. Zheng, F.S. Xiao, Metal-acid interfaces enveloped in zeolite crystals for cascade biomass hydrodeoxygenation, Appl. Catal. B 254 (2019) 560–568.
[13] T. Ishida, K. Kume, K. Kinjo, T. Honma, K. Nakada, H. Ohashi, T. Yokoyama, A. Hamasaki, H. Murayama, Y. Izawa, M. Utsunomiya, M. Tokunaga, Efficient decarbonylation of furfural to furan catalyzed by zirconia-supported palladium clusters with low atomicity, ChemSusChem 9 (2016) 3441–3447.
[14] P. Deng, J. Duan, F. Liu, N. Yang, H. Ge, J. Gao, H. Qi, D. Feng, M. Yang, Y. Qin, Y. Ren, **Atomic insights into synergistic nitroarene hydrogenation over nanodiamond-supported Pt_1−Fe_1 dual-single-atom catalyst**, Angew. Chem. Int. Ed. (2023) e202307853.
[15] S.H. Pang, C.A. Schoenbaum, D.K. Schwartz, J.W. Medlin, Directing reaction pathways by catalyst active-site selection using self-assembled monolayers, Nat. Commun. 4 (2013) 2448.

[16] H. Lv, H. Qin, M. Sun, F. Jia, B. Huang, B. Liu, Mesoporosity-enabled selectivity of mesoporous palladium-based nanocrystals catalysts in semihydrogenation of alkynes, Angew. Chem. Int. Ed. 134 (2022) 1–8.
[17] Y. Liu, E. Barath, H. Shi, J. Hu, D.M. Camaioni, J.A. Lercher, Solvent-determined mechanistic pathways in zeolite-H-BEA-catalysed phenol alkylation, Nat. Catal. 1 (2018) 141–147.
[18] M.A. Mellmer, C. Sener, J.M.R. Gallo, J.S. Luterbacher, D.M. Alonso, J.A. Dumesic, Solvent effects in acid-catalyzed biomass conversion reactions, Angew. Chem. Int. Ed. 53 (2014) 11872–11875.
[19] Z. Zhao, R. Bababrik, W. Xue, Y. Li, N.M. Briggs, D.-T. Nguyen, U. Nguyen, S. P. Crossley, S. Wang, B. Wang, D.E. Resasco, Solvent-mediated charge separation drives alternative hydrogenation path of furanics in liquid water, Nat. Catal. 2 (2019) 431–436.
[20] M.A. Mellmer, C. Sanpitakseree, B. Demir, P. Bai, K. Ma, M. Neurock, J.A. Dumesic, Solvent-enabled control of reactivity for liquid-phase reactions of biomass-derived compounds, Nat. Catal. 1 (2018) 199–207.
[21] J.S. Adams, A. Chemburkar, P. Priyadarshini, T. Ricciardulli, Y. Lu, V. Maliekkal, A. Sampath, S. Winikoff, A.M. Karim, M. Neurock, D.W. Flaherty, **Solvent molecules form surface redox mediators in situ and cocatalyze O_2 reduction on Pd**, Science 371 (2021) 626–632.
[22] L. Zhang, G. Meng, W. Zhang, X. Li, Z. Zhang, M. Yang, Y. Wu, D. Wang, Y. Li, Oriented conversion of a LA/HMF mixture to GVL and FDCA in a biphasic solvent over a Ru single-atom/nanoparticle dual-site catalyst, ACS Catal. 13 (2023) 2268–2276.
[23] Y. Deng, R. Gao, L. Lin, T. Liu, X.-D. Wen, S. Wang, D. Ma, Solvent tunes the selectivity of hydrogenation reaction over α-MoC, Catal., J. Am. Chem. Soc. 140 (2018) 14481–14489.
[24] V. Ranaware, R.G. Kurniawan, D. Verma, S.K. Kwak, B.C. Ryu, J.W. Kang, J. Kim, **Solvent-mediated selectivity control of furfural hydrogenation over a N-doped carbon-nanotube-supported Co/CoO_x catalyst**, Appl. Catal. B 318 (2022) 121838.
[25] G. Cheng, A. Jentys, O.Y. Gutiérrez, Y. Liu, Y.-H. Chin, J.A. Lercher, Critical role of solvent-modulated hydrogen-binding strength in the catalytic hydrogenation of benzaldehyde on palladium, Nat. Catal. 4 (2021) 976–985.
[26] I.K.M. Yu, F. Deng, X. Chen, G. Cheng, Y. Liu, W. Zhang, J.A. Lercher, Impact of hydronium ions on the Pd-catalyzed furfural hydrogenation, Nat. Commun. 13 (2022) 7154.
[27] J. Pang, J. Sun, M. Zheng, H. Li, Y. Wang, T. Zhang, Transition metal carbide catalysts for biomass conversion: A review, Appl. Catal. B 254 (2019) 510–522.
[28] Y. Yang, D. Rao, Y. Chen, S. Dong, B. Wang, X. Zhang, M. Wei, Selective hydrogenation of cinnamaldehyde over Co-based intermetallic compounds derived from layered double hydroxides, ACS Catal. 8 (2018) 11749–11760.
[29] D. Wang, X. Chen, D.G. Evans, W. Yang, **Well-dispersed Co_3O_4/Co_2MnO_4 nanocomposites as a synergistic bifunctional catalyst for oxygen reduction and oxygen evolution reactions**, Nanoscale 5 (2013) 5312–5315.
[30] Z. Jia, M. Peng, X. Cai, Y.-Q. Chen, X. Chen, F. Huang, L. Zhao, J. Diao, N. Wang, D. Xiao, X. Wen, Z. Jiang, H. Liu, D. Ma, Fully exposed platinum clusters on a nanodiamond/graphene hybrid for efficient low-temperature CO oxidation, ACS Catal. 12 (2022) 9602–9610.
[31] X. Xie, Y. Li, Z. Liu, M. Haruta, W. Shen, **Low-temperature oxidation of CO catalysed by Co_3O_4 nanorods**, Nature 458 (2009) 746–749.
[32] M. Kottwitz, Y. Li, R. Palomino, Z. Liu, G. Wang, Q. Wu, J. Huang, J. Timoshenko, S. Senanayake, M. Balasubramanian, D. Lu, R. Nuzzo, A. Frenkel, **Local structure and electronic state of atomically dispersed Pt supported on nanosized CeO_2**, ACS Catal. 9 (2019) 8738–8748.
[33] Y. Pan, L. Xu, L. Huang, W. He, H. Li, S. Wang, Z. Long, Z. Sun, Identification of active sites in Pt−Co bimetallic catalysts for CO oxidation, ACS Appl. Energy Mater. 4 (2021) 11151–11161.
[34] C. Sievers, Y. Noda, L. Qi, E.M. Albuquerque, R.M. Rioux, S.L. Scott, Phenomena affecting catalytic reactions at solid–liquid interfaces, ACS Catal. 6 (2016) 8286–8307.
[35] Q. Wang, J. Feng, L. Zheng, B. Wang, R. Bi, Y. He, H. Liu, D. Li, Interfacial structure determined reaction pathway and selectivity for 5-(hydroxymethyl)furfural hydrogenation over Cu-based catalysts, ACS Catal. 10 (2020) 1353–1365.
[36] Y. Yang, L. Chen, Y. Chen, W. Liu, H. Feng, B. Wang, X. Zhang, M. Wei, Selective hydrogenation of furfural on intermetallic compounds with outstanding catalytic performance, Green. Chem. 21 (2019) 5352–5362.
[37] Y. Zhu, W. Zhao, J. Zhang, Z. An, X. Ma, Z. Zhang, Y. Jiang, L. Zheng, X. Shu, H. Song, X. Xiang, J. He, Selective activation of C−OH, C−O−C, or C═C in furfuryl alcohol by engineered Pt sites supported on layered double oxides, ACS Catal. 10 (2020) 8032–8041.